Spectroscopy of HII Regions

Prof. Kelly Douglass

April 13, 2024

1 Nebulium

The brightest gaseious nebulae int he sky are made of starlight-ionized gas. They are subdivided into **HII regions**: sprawling irregular clouds associated with massive young stars and their formation regions; and **planetary nebulae**: compact, symmetrical shells of gas shed from dying, non-massive stars. Both varieties were subjects of the very first astronomical spectroscopic studies, soon after absoprtion lines in the Solar spectrum were identified in 1860, with emission lines in laboratory spectra of hot vapors of chemically-purified elements, by Robert Bunsen and Gustav Kirchoff[1] [8]. This was the first proof that the Sun is made of the same elements as the Earth. One of the first important follow-ups to the Bunsen- Kirchoff work was the identification on the Sun of the yet-undiscovered element Helium in 1868, which took a few more decades to find on Earth.

In contrast to the Sun, other stars, and the nebulae that we now call galaxies, HII regions and planetary nebulae show only emission spectra, including some bright lines unrepresented in any laboratory spectra. A set of particularly strong and pervasive unidentified nebular lines at 436 nm, 496 nm, and 501 nm was first seen around 1864 by William Huggins. With Helium as the precedent, and there being no reason to assume that celestial objects consist only of the terrestrial cast of elements, Huggins eventually took these lines to be the spectral signature of an element, Nebulium, that is found neither on Earth nor in the stars. This suggestion even survived the invention of the periodic table by Meyer and Mendeleev (1869)[2], which at the time of Huggins' work was rapidly filling up with elements found around the house. Failing to find a place in the table for Nebulium, people began discussing the possibility of "protoelements" of which Nebulium might be an example: that the nebulae are the progenitors of stars and planets, that nebulae are made of protoelements, and that the stars and planets are made from the elements, after those form *from* the protoelements. At the time, too little was known about the nature of atomic nuclei to rule out such possibilities.

This problem was still around in the mid-1920s for Ira Bowen to solve. Bowen measured many very high resolution vacuum ultraviolet spectra of second-row elements as a function of ionization state and used them to characterize the energy levels of these ions. He thereby discovered that the energy differences between the lowest-energy, metastable, states of several ordinary ions — some of whose permitted lines had been detected, albeit faintly, in nebulae — matched up perfectly with all of the spectral lines ascribed to Nebulium. Bowen noted that the forbidden nature of transitions between these metastable states, and the large rate of collisions even under the hardest vacuum that could be produced, would make it essentially impossible to detect the transitions directly in the laboratory. He also noted that, by the same token, these states could radiate brightly under the more rarified conditions already known by the hydrogen recombination line observations to exist in nebulae. Finally, he noted that the brightest Nebulium lines, with wavelengths 4363Å, 4959Å, and 5007Å in air, were strongly correlated in strength with the recombination lines of He^+. Bowen had found that the wavelengths of these lines were a match to O^{++}; this ion has excitation and ionization potentials similar to He^+ and should be expected to subsist in the same parts of nebulae [1, 2].

[1] Same Kirchoff whose rules you use to solve electrical circuit problems; same Bunsen whose burner heats your chemistry experiments. This was a hugely important result with influence throughout the sciences and humanities. Statues of both Bunsen and Kirchoff are found in Heidelberg, outside the buildings housing their departments: the highest accolade a scientist could receive, during the times before Nobel prizes and after absolute monarchies.

[2] Found most accessibly in the Dover reprint collection: Mendeleev, D.I. (2013), *Selected writings*, 1869–1905 (New York: Dover), paper #1. Mendeleev was Kirchoff's graduate student.

Thus, after a six-decade scientific life, Nebulium suddenly suffered the same fate as the aether. Soon, in the hands of such scientists as Zanstra, Menzel, Aller, and Bowen[3], the forbidden lines emitted by nebulae took their current place as the best probes of physical conditions and element abundances in the interstellar medium.

2 HII regions

Although visible light from young massive stars may escape in certain directions, their UV emission rarely does. Neutral hydrogen and especially dust are just too good at absorbing it. O stars have sufficient UV luminosity to dissociate molecules and ionize atoms for several light years around them. In turn, these atoms and ions can emit light with a much better chance than UV of escaping to a distant observer. The result is that the temperature of the ionized gas is determined by the balance between UV heating and the cooling emission by atoms, ions, and dust. The detection of this emission permits us to seek a solution to the inverse problem: what are the density, temperature, ionization state, and element abundances in the dissected gas that once belonged to the O star's natal molecular cloud.

This is a sport in which observational records are still broken by dramatic margins, despite 150 years of competition. Recently-commissioned inegral-field spectrographs[4], such as MUSE on one of ESO's 8-meter components of the Very Large Telescope in Chile, have produced essentially perfect data sets on the brightest HII regions. The MUSE results on the central 6'×9' of M 42 [14, 9], for example, cover $\lambda = 460$–937 nm at high dynamic range and with approximately Nyquist sampling, 0.2"×0.2"×0.085 nm spaxels. In this datacube, all the major features and lines in the nebula are spatially and spectrally resolved. Several abundant elements are detected in all of their significant ionization states. This yields a full accounting of temperature and density, ionization state, element abundance, bulk motion, and distinction between the HII region and the Herbig-Haro objects associated with younger stars behind the nebula. It only took a total of *five minutes* of exposure time to do all of this. Figures 1– 2 are samples of these results.

3 Recombination lines of Hydrogen

Once ionized, atoms recombine, usually into a highly excited state; once recombined, atoms emit a cascade of spectral lines, called **recombination lines**, as they decay to their ground state. The spectral lines emitted are all permitted, electric-dipole[5] transitions. The radiation rates — the average number of spontaneous transitions per unit time, a.k.a. **Einstein A-coefficients** — of such transitions are of the order of once per microsecond, much faster than the rate at which atoms or ions collide with each other in interstellar gas. So, the vast majority of neutral H atoms are in the ground state, and the emission rate for a given recombination line depends only on the rate of recombination times a factor that accounts for the branching among different allowed paths in the cascade. All but recombinations directly into the ground ($n = 1$) state, that is: this results in the emission of a photon with energy greater than the ionization energy that will be absorbed,

[3] In her revolutionary work on the relative abundances of elements in stellar atmospheres (PhD thesis, Harvard, 1925, and [10]), Cecilia Payne uncharacteristically bowed in one respect to the prejudices of senior astronomers, prominently Henry Norris Russell's. Though it was a robust result of her analysis that H and He were vastly more abundant in stars than the other elements, despite not being so on Earth, Payne concluded that, "...the stellar abundance deduced for these elements is improbably high, and is almost certainly not real." It must have cheered her up that, soon afterward, her result was strongly supported by those on gaseous nebulae. Bowen's conclusion, for example [3] "It is therefore evident that all elements except H and He are very rare in the nebulae."

[4] Also invented by Bowen [4]

[5] Too quickly: In first-order time-dependent perturbation theory, the rate of spontaneous transitions between states j and i are proportional to the square modulus of the matrix element between these states of the interaction Hamiltonian V, $|\langle j|V|i\rangle|^2$. In turn, the interaction Hamiltonian for light and an atom contains a factor $e^{-i\vec{\kappa}\cdot\vec{r}}$ that represents a plane wave of light; here, $|\vec{\kappa}| = 2\pi/\lambda$ is the wavenumber of the light. The wavelength of light for ultraviolet wavelengths and longward is many orders of magnitude larger than the extent of an atom's electron states in r, so it is appropriate to expand the exponential in a power series ($e^{-i\vec{\kappa}\cdot\vec{r}} = 1 - i\vec{\kappa}\cdot\vec{r} + \ldots$) and keep only the lowest-order term that gives a nonvanishing matrix element $\langle j|V|i\rangle$. Together with the rest of the interaction Hamiltonian, the first term in this series expansion gives rise to a matrix element proportional to $q_e \sum_n \langle j|\vec{r}_n|i\rangle$, the total electric dipole moment of the atom's n electrons. Transitions between states j and i for which this term gives the rate are therefore called electric dipole transitions. Conservation of angular momentum and the spin-1 nature of photons — or, if you prefer, orthogonality of the Legendre polynomials — dictate the selection rule for electric dipole transitions in single-electron atoms: $\Delta\ell = \pm 1$, where ℓ is the orbital angular momentum quantum number.

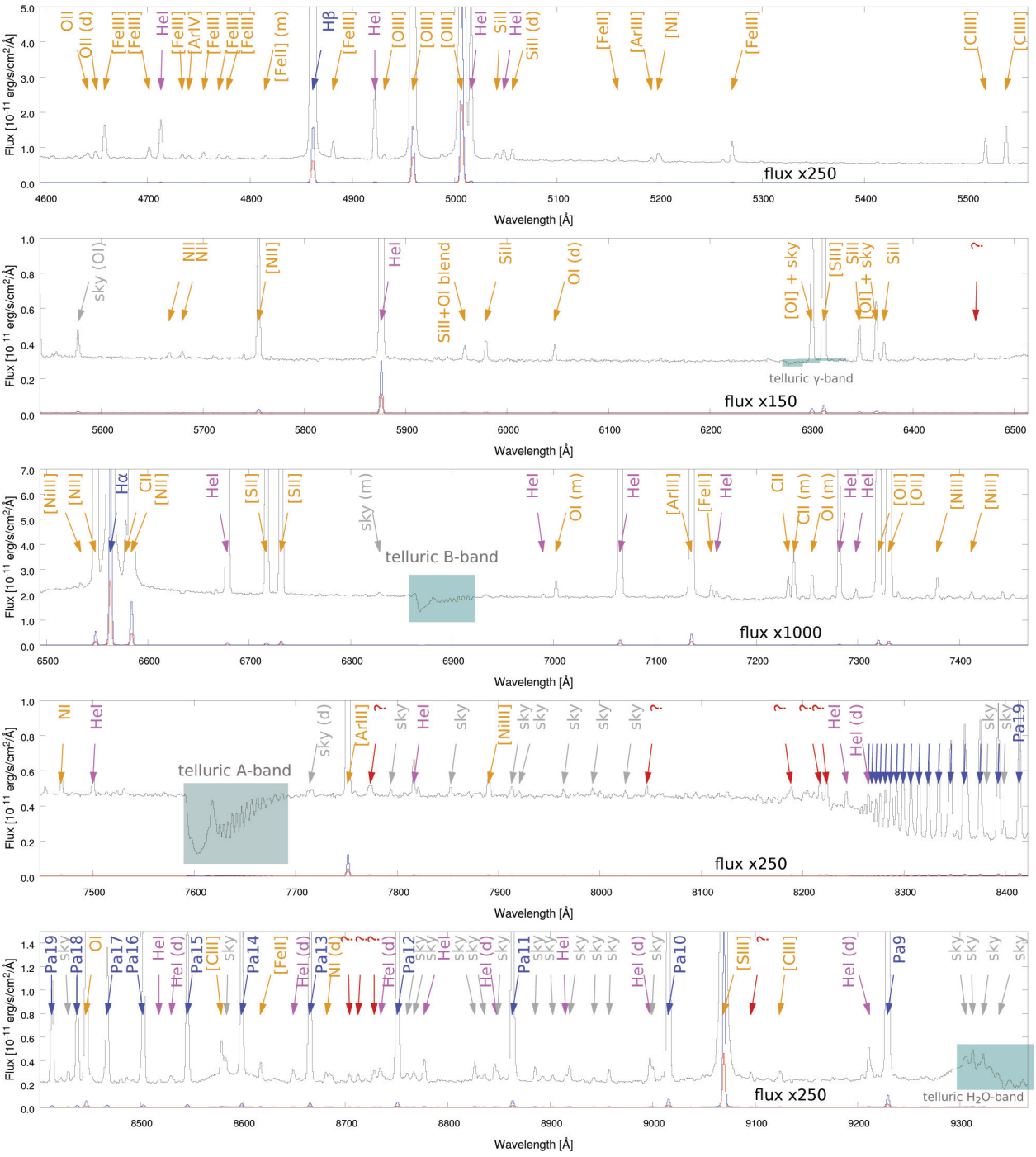

Figure 1: MUSE spectra [14] of a couple of east-west stripes of M 42, shown in blue and red; and a magnified version of the latter spectrum, in black with scale features given in each frame, to show fainter lines. The molecular bands labeled A and B are from oxygen in Earth's atmosphere. Ten "U lines" (unidentified) are also present, surprisingly numerous at this late date. They are probably not due to Nebulium 2.0; most are unidentified due to multiple plausible identifications.

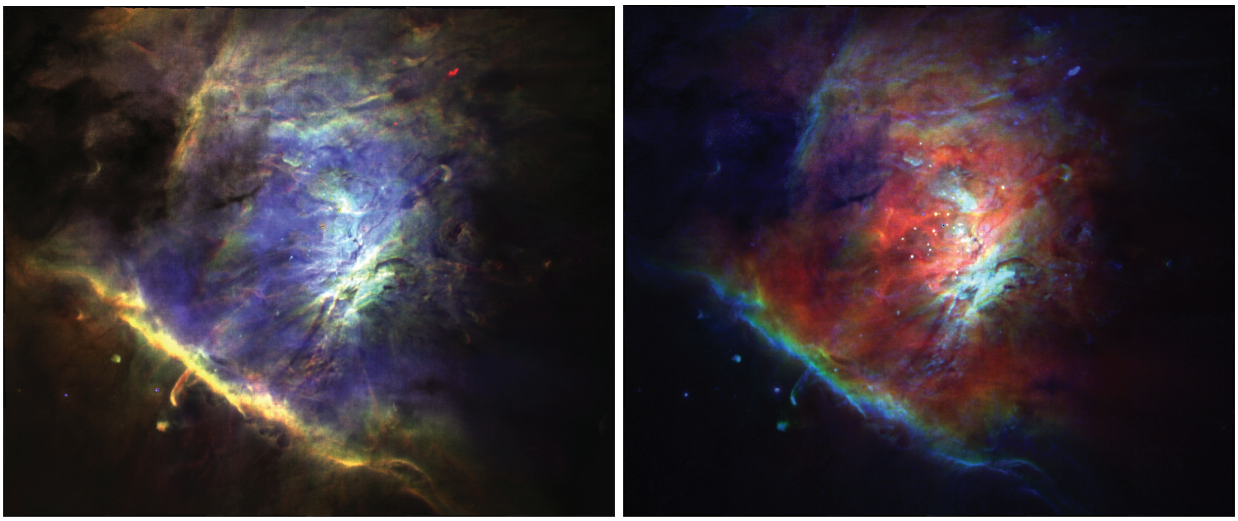

Figure 2: MUSE spectral-line composite images of M 42 [14]. Both are corrected for extinction, using images of the Balmer decrement. Left: RGB = [SII] 6731Å, [NII] 6584Å, Hβ. Right: [OIII] 5007Å, [OII] 7320Å, [OI] 6300Å.

practically on the spot, by a neighboring neutral hydrogen atom. Recombinations that immediately lead to ionizations do not really count as recombinations: they are left out of the rate coefficients that we use for HII region analysis.[6]

The rate of recombination also depends on the densities of electrons and ions that are available to recombine. Recombination and branching, leading to a transition between states j and i, are usually characterized by an **effective recombination rate coefficient** α_{ji}, such that the rate at which these transitions happen per unit volume is given by $\alpha_{ji} n_e n_{\rm ion}$. The αs are calculated (quantum-mechanically) and are known with a very high accuracy for simple, well-characterized atoms like hydrogen. They depend weakly on temperature and even more weakly on density.

Given an effective recombination rate, the total power per unit volume, J_{ji}, emitted in spectral line radiation for states j and i, is simply the product of this rate and the photon energy:

$$J_{ji} = \frac{hc}{\lambda_{ji}} \alpha_{ji} n_e n_{\rm ion}$$

Table 1 is a list of wavelengths[7] and recombination rate coefficients [7, 13][8] times hc/λ for hydrogen lines connecting lower-energy states at temperature $T = 10^4$ K and low density. Transitions to the $2s$ or $2p$ state, called the **Balmer series**, lie at visible wavelengths and are labeled Hα, Hβ,... from long wavelength to shorter.

We presume that the atoms emit isotropically (uniformly into 4π steradians). We are safe in assuming that nebulae are optically thin (transparent) to recombination-line radiation, except for those that connect to the ground, $n = 1$ state[9]. With these caveats, the recombination line intensity, I_{ji} (power per unit area per unit solid angle), at the surface of the nebula is

$$I_{ji} = \frac{1}{4\pi} \int J_{ji}\, ds = \frac{hc}{4\pi\lambda_{ji}} \int \alpha_{ji} n_e n_{\rm ion}\, ds \qquad (1)$$

where the integration is over the distance s along the line of sight through the nebula. In the case of hydrogen, the ion density is that of free protons, n_p. Since α_{ji} depends only weakly on density and temperature, it

[6] The leaving out of recombinations directly into the ground state is called **Case B recombination**; this case will apply to all of the recombination rate coefficients that we list in the following.

[7] https://physics.nist.gov/PhysRefData/ASD/lines_form.html

[8] In [13], the results [7] are extended to the kappa electron energy distribution. The easiest way to get the former reference's data in electronic form is to use the latter reference at the largest values of κ.

[9] Because of hydrogen's large abundance and the pile-up of the population in the ground state, nebulae are always extremely optically thick (opaque) in transitions to the ground, $1s$, state: the **Lyman series**.

j	Balmer $i=2$	Paschen $i=3$	Brackett $i=4$	Pfund $i=5$	Humphreys $i=6$
			λ, vacuum [μm]		
10	0.37970	0.90125	1.73575	3.03756	5.12588
9	0.38344	0.92266	1.81693	3.29521	5.90501
8	0.38881	0.95435	1.94404	3.73853	7.49843
7	0.39691	1.00467	2.16495	4.65126	12.36519
6	0.41007	1.09352	2.62445	7.45582	
5	0.43394	1.28147	4.05008		
4	0.48601	1.87461			
3	0.65611				
			$(hc/\lambda)\alpha_{ji}$ [erg/cm^3/s]		
10	6.55×10^{-27}	2.28×10^{-27}	1.13×10^{-27}	6.56×10^{-28}	4.18×10^{-28}
9	9.03×10^{-27}	3.14×10^{-27}	1.56×10^{-27}	9.10×10^{-28}	5.79×10^{-28}
8	1.30×10^{-26}	4.52×10^{-27}	2.26×10^{-27}	1.32×10^{-27}	8.31×10^{-28}
7	1.96×10^{-26}	6.85×10^{-27}	3.44×10^{-27}	2.00×10^{-27}	1.21×10^{-27}
6	3.20×10^{-26}	1.12×10^{-26}	5.62×10^{-27}	3.15×10^{-27}	
5	5.78×10^{-26}	2.02×10^{-26}	9.91×10^{-27}		
4	1.24×10^{-25}	4.18×10^{-26}			
3	3.54×10^{-25}				

Table 1: Visible and infrared hydrogen recombination lines, $T = 10^4$ K.

can be taken out of the integral to good approximation. The remaining integral $\int n_e n_p \, ds$ is often called the nebular **emission measure**.

4 Extinction and its correction

The intensity received by a distant observer suffers an additional factor of $e^{-\tau(\lambda_{ji})}$: extinction, primarily due to absorption by cold foreground dust. This must be corrected before analysis. If two hydrogen recombination lines are observed, the extinction can be determined both accurately and independently of the details of the nebula, due to the weak dependence of the αs on density and temperature. The two longest-wavelength Balmer series lines, Hα and Hβ, often serve this purpose. Their intensity ratio, called the **Balmer decrement**, is $I(\mathrm{H}\alpha)/I(\mathrm{H}\beta) \cong 2.86$ without extinction; any upward departure from this ratio can be ascribed to extinction and serves to measure the reddening, $e^{-\tau(\mathrm{H}\alpha)+\tau(\mathrm{H}\beta)}$. From this and the experimental results on interstellar dust, the foreground extinction can be obtained, as in Figure 3. When calculating the foreground extinction, keep in mind the following relationships:

$$A_\lambda = 2.5 \log\left(\frac{I_0(\lambda)}{I(\lambda)}\right) \tag{2}$$

where A_λ is the foreground extinction at wavelength λ, and

$$R_\lambda \equiv \frac{A_\lambda}{E(B-V)} \tag{3}$$

where R_λ is the extinction ratio at wavlength λ. Typically, A_λ/A_V is an empirical relationship fit to detailed observations.

5 Forbidden lines

In a multielectron atom or ion, the lowest-energy electron configuration gives rise to several **multiplets**: groups of states with the same total orbital and spin angular momentum, separated from other multiplets

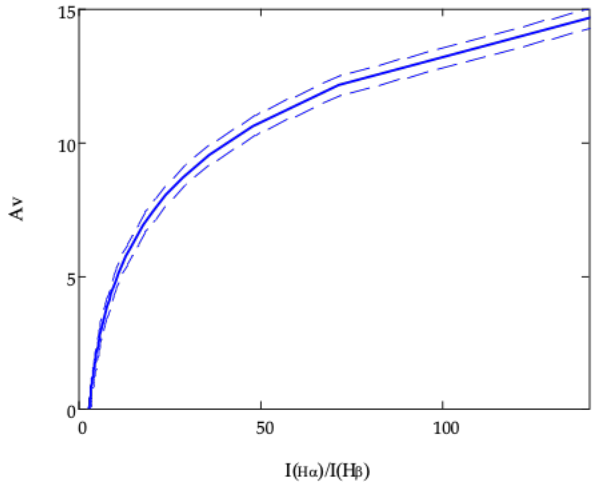

Figure 3: A_V in magnitudes, plotted against the Balmer decrement, $I(\mathrm{H}\alpha)/I(\mathrm{H}\beta)$, with hypothetical $\pm 10\%$ uncertainty in the decrement indicated by the shaded region. The decrement is evaluated at low density and $T = 10^4$ K, as in Table 1. Extinction and dust grain properties are from [15] for a total-to-selective extinction ratio of $R_V \equiv A_V/E(B-V) = 5.5$.

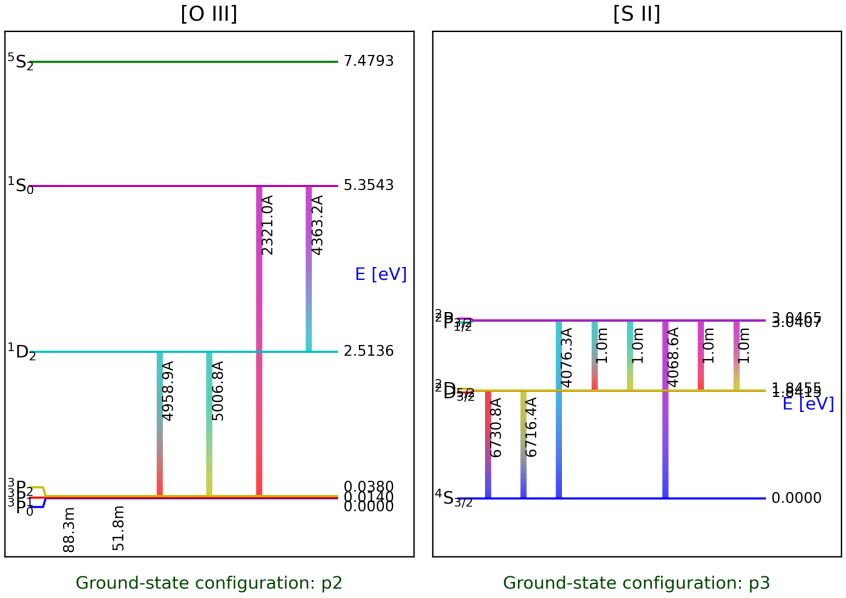

Figure 4: Lowest five states of O^{++} and S^{+}, all of which are metastable, and the stronger of the forbidden transitions connecting them.

by energies of order 0.1–1 eV[10] In the lighter-weight atoms in which the indices of total orbital and spin angular momenta, L and S, are good quantum numbers[11], transitions among these multiplets, and the states within them, are **forbidden**. Their Einstein A-coefficients are many orders of magnitude smaller than those of lines of similar wavelength linking different electronic configurations, such as recombination lines. Forbidden transitions are of magnetic-dipole or electric-quadrupole nature, rather than electric dipole like recombination lines[12]. States for which all transitions to lower-energy states are forbidden are called **metastable**. Figure 4 is a diagram of the lowest-energy multiplets of O^{++} and S^{+}, two ions common in HII regions, along with the brighter visible and infrared lines connecting their states. All of these states are metastable and linked only by forbidden transitions, as is common among multielectron atoms.

For elements of the first three rows of the periodic table, or their ions, electronic wavefunctions are well characterized. The matrix elements for magnetic dipole and electric quadrupole transitions, and thus their A-coefficients, can be accurately calculated. If the density of an ion in state j is n_j, then the power in transition $j \rightarrow i$ emitted from a unit volume is

$$J_{ji} = \frac{hc}{\lambda_{ji}} A_{ji} n_j \tag{4}$$

Here, A_{ji} is the Einstein A-coefficient for the transition.[13] As they are for recombination lines, nebulae are optically thin (transparent) to forbidden-line radiation. In analogy with Equation 1, the intensity emitted from the nebula, at the nebula's surface, is

$$I_{ji} = \frac{hc}{4\pi\lambda_{ji}} A_{ji} \int n_j \, ds \tag{5}$$

The integral of density along the line of sight, $N_j = \int n_j \, ds$, is often called the **column density** of the ion in state j. We do not yet know how n_j relates to the total density n of the ion; this is the subject of the next few sections.

As before, the intensity received by a distant observer suffers an additional factor of $e^{-\tau(\lambda_{ji})}$ from extinction by cold foreground dust. None of the forbidden lines that are bright in HII regions are particularly useful in determining extinction, but we will meet some in the next memo in this series, on [FeII] emission from shocked gas.

[10]The classification scheme normally used for the states of elements H through Fe is **Russell-Saunders**, or **LS, coupling**. In this scheme, the electron spins and directions are added to get a total electron spin quantum number S, their orbital angular momenta to get a total orbital angular momentum quantum number L, and the vector sum of S and L to get the total angular momentum quantum number J. For example, O^{++} has electron configuration [He]$2s^2 2p^2$. The spin of the two p electrons can be arranged either in a triplet state or a singlet, so O^{++}'s total spin quantum number S can be either 1 or 0, respectively. Each electron has one unit of orbital angular momentum, so the total orbital angular momentum quantum number L can be 0, 1, or 2. The spin triplet state has even symmetry: interchanging the electron coordinates does not change the sign of the spin part of the wavefunction. By the same token, the odd-symmetry, spin-singlet state changes sign on electron-coordinate interchange. However, the total wavefunction must change sign on interchange of the electrons if they are to obey Fermi-Dirac statistics. The $L = 1$ orbital-angular-momentum state changes sign on interchange, as it is an odd function of the spatial coordinates; the others do not. Thus, the $S = 1$ states can only have $L = 1$, while the $L = 0$ and 2 states must have $S = 0$. The choices for total angular momentum quantum number J are 0, 1, and 2 for the $L = 1$ states, while the $L = 0$ and 2 states must have $J = 0$ and 2, respectively. It is customary to label these states ${}^{2S+1}L_J$, and to use the electron-orbit-reminiscent letters S, P, and D to stand for $L = 0, 1$, and 2. So the five states of [He]$2s^2 2p^2$ are ${}^1S_0$, ${}^1D_2$, ${}^3P_2$, ${}^3P_1$, and ${}^3P_0$.

[11]A good quantum number corresponds to a rigorously conserved quantity. Of course, total angular momentum is such a quantity. L and S are often pretty good quantum numbers, but in principle their corresponding angular momenta are not individually conserved. LS coupling becomes less useful past the first three rows of the periodic table.

[12]In strict LS coupling, the selection rules for electric dipole transitions are $\Delta S = 0$; $\Delta L = \pm 1$, or 0; and $\Delta J = \pm 1$, or 0, but no $J = 0 \rightarrow 0$. Magnetic dipole transitions have no separate selection rule for the S — that is, any ΔS is OK for such a transition — but require $\Delta L = 0$, $\Delta J = \pm 1$. For electric quadrupole transitions, only J has a selection rule: $\Delta J = \pm 2, \pm 1, 0$, but no $0 \rightarrow 0$, $1/2 \rightarrow 1/2$, or $0 \rightarrow 1$.

[13]Forbidden transitions being too weak to measure in the laboratory, their A-coefficients must be calculated from the electronic wavefunctions of the ions, which in turn can be accurately constrained by experimental determination of the energies of these states. The more simple the atom or ion, the more accurately its wavefunctions are known. For elements of the first three rows of the periodic table (like O and S), calculations of A-coefficients have changed very little over the last three decades, despite much more complex calculations and revolutionary changes in computing power that have made them possible, so the A-coefficient accuracy is probably very good.

6 Collisional de-excitation

Unlike recombination lines, forbidden lines are emitted because their upper states are excited by collisions, mostly with electrons within the ionized gas. This makes the forbidden lines crucially important for the thermal state of nebulae: thermal energy is converted thereby, efficiently, to radiation which escapes directly to outer space, cooling the nebula.

Let us consider an oversimplified version of a collision between a positive ion with charge Ze and an electron, incident on the ion at speed v and aimed a distance b from the ion. Suppose that, if the electron got sufficiently close to the ion, it could transfer some of its kinetic energy to the ion and cause it to change states: an inelastic collision. Much lighter than the ion, the electron moves much faster; the ion is essentially at rest during the interaction. Electrostatic attraction bends the electron's path toward the ion,[14] as shown in Figure 5. It passes within a distance r_0 of the ion, now traveling at speed v_0. Energy and angular momentum conservation gives us

$$\frac{1}{2}m_e v^2 = \frac{1}{2}m_e v_0^2 - \frac{Ze^2}{r_0} \qquad \text{and} \qquad m_e v b = m_e v_0 r_0 \tag{6}$$

Use the latter expression to eliminate v_0 from the former expression, and rearrange to solve for $\sigma = \pi b^2$:

$$\sigma \equiv \pi b^2 = \pi r_0^2 \left(1 + \frac{2Ze^2}{mv^2 r_0}\right) \tag{7}$$

For this collision to result in a transition among the ion's states, r_0 must be small enough to give sufficient overlap of wavefunctions. If we take this to be of order the Bohr radius, $r_0 = a_0 = \hbar^2/m_e e^2$, or smaller, and if we take the initial electron kinetic energy to be the thermal energy, $3kT/2$, at a typical HII region of $T = 10^4$ K, we see that $2Ze^2/mv^2 r_0 \gtrsim 20Z \gg 1$, so the 1 in the brackets above can be neglected:

$$\sigma \approx \frac{2\pi Z e^2 a_0}{m_e v^2} = \frac{\pi\hbar^2}{m_e^2 v^2} 2Z \tag{8}$$

The **cross section**, σ, is the effective area of the atom for intercepting electrons and undergoing that transition. If the electron density is n_e and the electrons move at typical speed v, then the flux of electrons (electrons per unit area) in one direction is $n_e v$. If the density of ions is n, then the rate R at which these inelastic collisions occur per unit volume is

$$R = n_e v \sigma n = n_e n v \frac{\pi\hbar^2}{m_e^2 v^2} 2Z \tag{9}$$

When one casts this situation as a quantum-mechanical problem — which turns out to be very challenging — the resulting cross section takes a similar form:

$$\sigma_{ji} = \frac{\pi\hbar^2}{m_e^2 v^2} \frac{\Omega_{ji}(v)}{g_j} \tag{10}$$

where $\Omega_{ji}(v)$ is the dimensionless **collision strength** that embodies the integral of the time-dependent matrix elements; j and i are the states of the ion; and g_j is the statistical weight of state j. $g_j = 2J + 1$ if the state has total angular momentum quantum number J, as this is the number of values of J_z. Usually, just the strengths for collisional de-excitations are calculated: j is the higher energy of the two states. The number of collisionally-induced transitions $j \to i$ per unit volume, $R_{ji}(v)$, is

$$R_{ji}(v) = n_e n_j v \sigma_{ji}(v) = n_e n_j v \frac{\pi\hbar^2}{m_e^2 v^2} \frac{\Omega_{ji}(v)}{g_j} \tag{11}$$

[14] A proton in the same medium would have the same thermal energy as the electron, but it would be steered away from the ion; because of the exponential radial dependence of atomic wavefunctions, the resulting collisional transition rate would be vastly smaller than that with electrons. That is why you will only ever see electron collisions discussed in the context of HII regions.

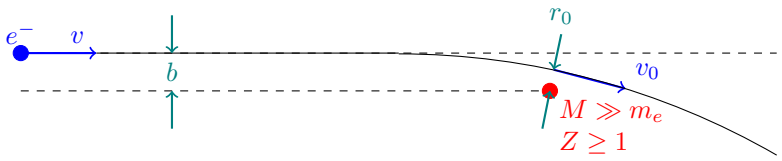

Figure 5: Electron-ion collision in ionized gas.

In thermal equilibrium at temperature T,[15] the Maxwell-Boltzmann distribution applies to electron speeds:

$$f(v) = \left(\frac{m_e}{2\pi kT}\right)^{3/2} 4\pi v^2 e^{-m_e v^2/2kT} \tag{12}$$

so the net rate of transitions per unit volume is

$$\langle R_{ji} \rangle = n_e n_j \int_0^\infty v \sigma_{ji}(v) f(v)\, dv = n_e n_j \sqrt{\frac{2\pi}{kT}} \frac{\hbar^2}{m_e^{3/2}} \frac{\Gamma_{ji}(T)}{g_j} \tag{13}$$

where $\Gamma_{ji}(T)$ is the dimensionless *effective* collision strength. The $\Gamma_{ji}(T)$ are what gets tabulated in the literature, on a grid of temperatures in a useful range, dense enough to interpolate accurately in codes.

7 Detailed balance in thermal equilibrium, and collisional excitation

The next steps in the use of collisional cross sections are to calculate the metastable-state populations that result from the combined effect of collisional de-excitation, excitation, and radiation. This starts with the definition of a collisional de-excitation rate coefficient, $\gamma_{ji}(T)$:

$$\gamma_{ji} = \sqrt{\frac{2\pi}{kT}} \frac{\hbar^2}{m_e^{3/2}} \frac{\Gamma_{ji}(T)}{g_j} = \frac{8.629 \times 10^{-6}\ \mathrm{cm^3\ s^{-1}\ K^{1/2}}}{\sqrt{T}} \frac{\Gamma_{ji}(T)}{g_j} \tag{14}$$

Upward, collisional excitation, rate coefficients are obtained from the downward ones by application of detailed balance in thermal equilibrium, as follows. If in addition to thermal equilibrium prevailing among translational motions, the states were populated according to thermal equilibrium at the same temperature as the free electrons, there would be **detailed balance** among the collisional transitions between any two states: $\langle R_{ij} \rangle = \langle R_{ji} \rangle$. With $Z(T)$ as the partition function (total number of electronic states; not to be confused with ion charge as above) and n as the total density of this ion, detailed balance would imply

$$n_e n_i^{TE} \gamma_{ij}(T) = n_e n_j^{TE} \gamma_{ji}(T) \tag{15}$$

$$n_e \frac{n g_i e^{-E_i/kT}}{Z(T)} \gamma_{ij}(T) = n_e \frac{n g_j e^{-E_j/kT}}{Z(T)} \gamma_{ji}(T) \tag{16}$$

$$\gamma_{ij}(T) = \gamma_{ji}(T) \frac{g_j}{g_i} e^{-\Delta E_{ji}/kT} \tag{17}$$

Since the densities have dropped out of the expression, the **resulting relation between γ_{ij} and γ_{ji} applies at any density**, whether the states are populated thermally or not. So, it suffices for the quantum calculations to cover the de-excitations, and for us to obtain the excitations easily from detailed balance.

[15] Always ask, "the temperature of what?" and "can they even have a temperature?" Here, we mean the temperature of the electrons and protons (ionized hydrogen). Their motions are in thermal equilibrium because they efficiently share their kinetic energy and momentum *via* collisions like that in Figure 5. In turn, this is because collisions among them are much more frequent than any other process in which they participate. For example: suppose an ionized cloud of diameter $r = 1$ pc had density $n_e \approx n_p = 1\ \mathrm{cm^{-3}}$ and typical electron speed $v = 1$ km/s. The proton cross section for electron collisions would be $\sigma = 8.4 \times 10^{-10}\ \mathrm{cm^2}$, and the typical time between collisions $1/n_e \sigma v \approx 10^4$ s. This is very short, astrophysically speaking: the cloud-crossing time, for example, is $r/v \approx 10^6$ yrs, more than nine orders of magnitude longer. So the electrons and protons certainly collide often enough that their motions represent thermal equilibrium, and we can describe them with a temperature.

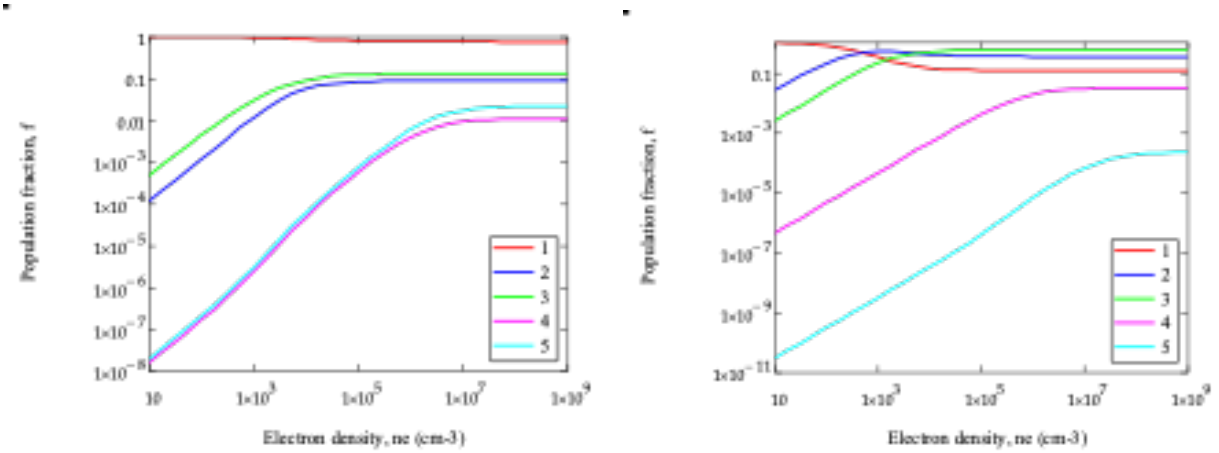

Figure 6: Population fractions, f_i, for the metastable states of S^+ (left) and O^{++} (right) at $T = 10^4$ K. as a function of electron density n_e. The curves are labeled in increasing order of the energy of the states.

8 Critical density for collisional de-excitation

A useful marker of the electron-density sensitivity of a collisionally-excited spectral line is the **critical density**, n_C, of its upper state, defined as the ratio of sums of A-coefficients and collisional excitation rate coefficients involving this state:

$$n_{Cj}(T) = \frac{\sum_{i<j} A_{ji}}{\sum_{i \neq j} \gamma_{ji}(T)} \tag{18}$$

That is, the critical density is the electron density for which radiative and collisional decay rates are equal. Table 2 is a list of critical densities for the states in Figure 4, for electron collisions at $T = 10^4$ K.

Ground states do not decay, of course, so they do not have critical densities.

9 Multilevel collisional excitation

This section can be skipped at first reading. The material is not difficult, but the linear algebra is tedious. Code is available on request which may eliminate the need to stare at the equations wondering how you got the array indices wrong.

The partition of the population of ions over the various states is determined under the assumption that the densities have reached a **steady state**.[16] Assuming only optically-thin media, the rate of transitions *out* of state j equals the rate of transitions *in*:

$$n_j \sum_{i \neq j} n_e \gamma_{ji} + n_j \sum_{i<j} A_{ji} = \sum_{i \neq j} n_i n_e \gamma_{ij} + \sum_{i>j} n_i A_{ij} \tag{19}$$

This is a system of equations that we must solve for the unknown n_j in order to calculate line intensities (Equation 5). Since $\gamma_{jj} = 0$, and since $A_{ji} = 0$ unless state i has a lower energy than state j, we will assume that the states are indexed in order of increasing energy and allow all of the sums to extend over all bounded states. The densities in all of the levels add up to the density of the ion:

$$\sum_j n_j = n \tag{20}$$

Write $f_j = n_j/n$ and rearrange slightly to get

$$f_j \sum_i (n_e \gamma_{ji} + A_{ji}) - \sum_i f_i (n_e \gamma_{ij} + A_{ij}) = 0 \tag{21}$$

[16] Steady state is not the same as thermal equilibrium. Some or all of the states of the ion in question may have populations very far from their thermal equilibrium values, at the temperature of the surrounding electron gas.

S^+		O^{++}	
State	n_C (cm^{-3})	State	n_C (cm^{-3})
$^2D_{3/2}$	2.82×10^3	$^3P_1$	5.01×10^2
$^2D_{5/2}$	1.26×10^3	$^3P_2$	3.53×10^3
$^2P_{1/2}$	1.19×10^6	$^1D_2$	6.92×10^5
$^2P_{3/2}$	2.24×10^6	$^1S_0$	2.43×10^7

Table 2: Critical densities for S^+ and O^{++}

$$\sum_j f_j = 1 \tag{22}$$

The second term in Equation 21 is a matrix multiplication: the inner product of a second-rank tensor, $n_e\gamma_{ij} + A_{ij}$, with a vector f_i. The first term is of the form f_jC_j, which could also be thought of as a matrix multiplication if C_j were the diagonal elements of a matrix with no non-zero off-diagonal elements. Thus, we can use a Kronecker delta to represent the diagonal matrix, and rewrite Equation 21 as

$$\sum_i f_i\delta_{ij}\sum_k(n_e\gamma_{jk} + A_{jk}) - \sum_i f_i(n_e\gamma_{ij} + A_{ij}) = 0 \tag{23}$$

or

$$\sum_i f_iD_{ij} = 0 \qquad D_{ij} = \delta_{ij}\sum_k(n_e\gamma_{jk} + A_{jk}) - n_e\gamma_{ij} - A_{ij} \tag{24}$$

This is a linear system in the unknowns f_i, as many equations as unknowns. However, the equations are not linearly independent: clearly, the coefficient matrix D_{ij} has zero determinant. For one of these equations, we can substitute the normalization condition, Equation 22. Suppose that we replace the pth one, creating a new coefficient matrix D'_{ij}:

$$D'_{pj} = 1 \qquad D'_{i\neq p,j} = D_{ij} \tag{25}$$

With this substitution, Equation 24 becomes

$$\sum_i f_iD'_{ij} = \delta_{jp} \tag{26}$$

There are many efficient ways to solve this system for f_j. One *inefficient* way to do so is to simply calculate the inverse of the coefficient matrix and multiply through:

$$f_k = \sum_j \delta_{pj}D'^{-1}_{jk} = D'^{-1}_{pk} \tag{27}$$

For the temperatures and densities encountered in HII regions, one may neglect the population in excited electron configurations, leaving only the metastable states of the lowest-energy configuration: five states or so, as in Figure 3. It is not prohibitively slow to invert that small a coefficient matrix; most of us do it that way, using matrix-inversion routines native to our programming environment.

Figure 6 is a set of solutions of Equation 26 for the metastable states of S^+ and O^{++}. Note in this figure that the curves all level off at high density, when the states have reached their thermal-equilibrium population fractions. Note also that each curve levels off at an electron density a little larger than the critical density listed in Table 2.

10 Derivation of physical parameters from line-intensity observations

We can measure recombination and forbidden-line intensities from HII regions. Using these, we can extract the density, temperature, ionization state, and elemental abundances in the nebula, and the foreground

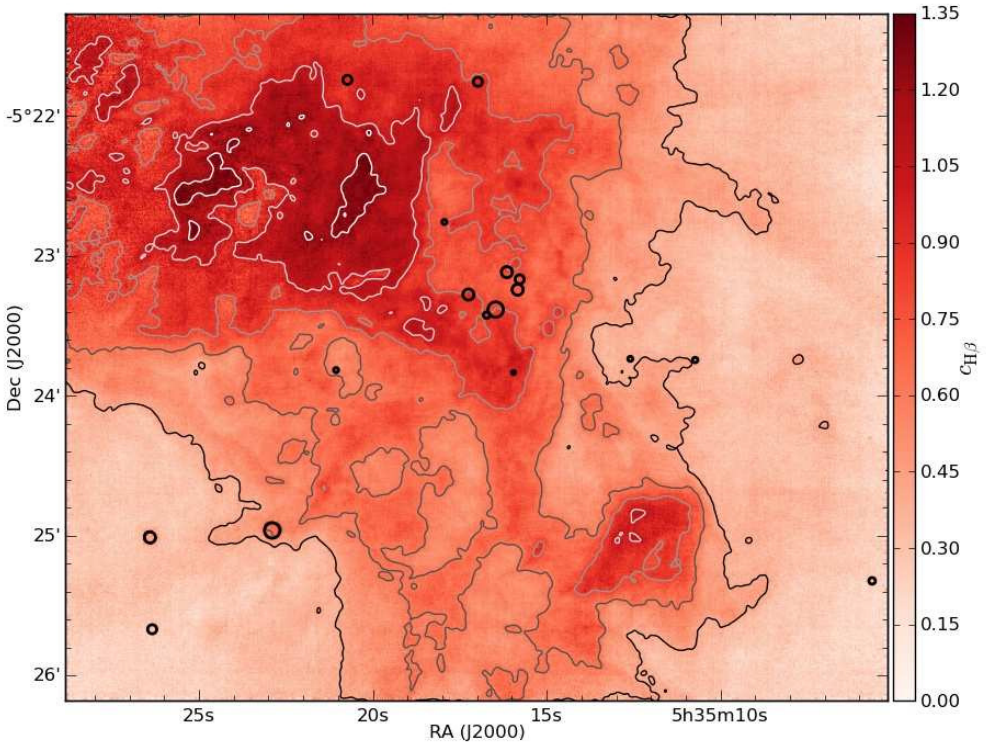

Figure 7: Extinction toward M 42, from MUSE observations of the Balmer decrement [14], expressed as $c_{H\beta} = \tau_{H\beta}/\ln(10)$. The full range of $c_{H\beta}$ corresponds to $A_V = 0.9$–2.7 mag.

extinction, from Equations 1, 5, and 27:

$$I_{ji} = e^{-\tau(\lambda_{ji})} \frac{hc}{4\pi\lambda_{ji}} \int \alpha_{ji} n_e n_p \, ds \qquad \text{for recombination lines, and} \tag{28}$$

$$= e^{-\tau(\lambda_{ji})} \frac{hc}{4\pi\lambda_{ji}} A_{ji} \int f_j n \, ds \qquad \text{for forbidden lines,} \tag{29}$$

where, as in the previous section, n is the density of the ion producing the forbidden line, and f_j is the fraction of the ions in the upper state j. We write the foreground extinction factor in the sensible exponential form, though of course it is conventional to express extinction in magnitudes.

There are several approaches to the use of Equations 28–29 with visible and near-infrared data. One can get surprisingly far, though, with the simplest approach that would spring to mind: a uniform plane-parallel slab of ionized gas, in general a different one for every angular resolution element in your images or along your spectrograph slit.

10.1 Uniform ionized cloud, 1D

With the one dimension along the line of sight, this assumption simplifies the integrals:

$$I_{ji} = e^{-\tau(\lambda_{ji})} \frac{hc}{4\pi\lambda_{ji}} \alpha_{ji} n_e N_p \qquad \text{for recombination lines, and} \tag{30}$$

$$= e^{-\tau(\lambda_{ji})} \frac{hc}{4\pi\lambda_{ji}} A_{ji} f_j N \qquad \text{for forbidden lines,} \tag{31}$$

where the Ns are column densities of protons and ions: density integrated along the line of sight, as in Section 5 above. In the following, we will assume that I_{ji} refers to total line flux, but the analysis does not differ substantially if the line profiles are spectroscopically resolved. The steps, in order:

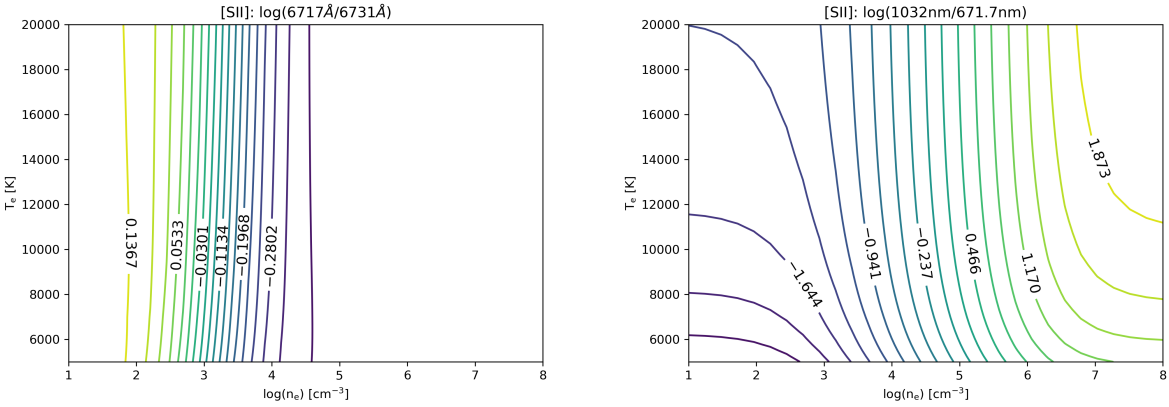

Figure 8: Contours of logarithms of [SII] line-intensity ratios, 671.7 nm / 673.1 nm (left) and 1032 nm / 671.7 nm (right), plotted against n_e and T.

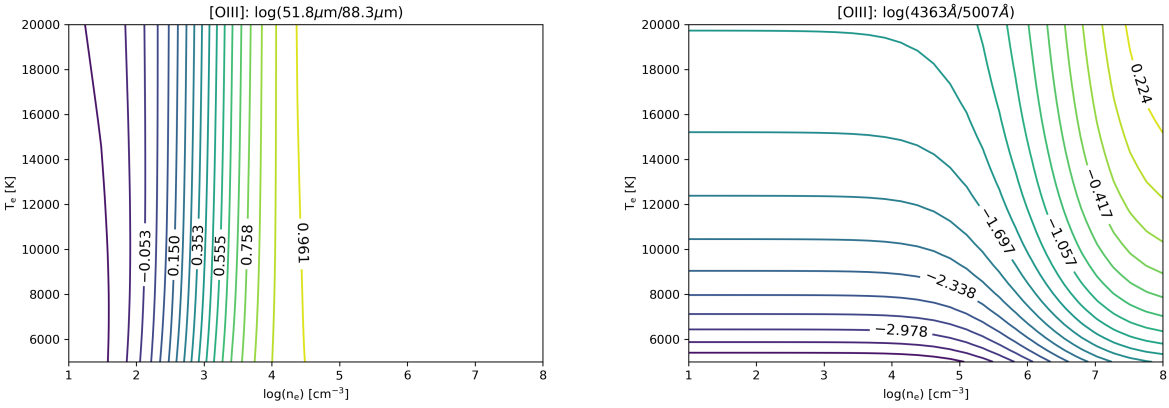

Figure 9: Contours of logarithms of [OIII] line-intensity ratios, 51.82 μm / 88.35 μm (left) and 436.3 nm / 500.7 nm (right), plotted against n_e and T.

1. **Determine the foreground extinction**, using a pair of hydrogen recombination lines: the Balmer decrement, for example, as in Figure 3. HII regions are associated with molecular clouds, so the extinguishing dust grains are usually on the high end of the range of total/selective extinction ratio R. In Figure 3, we used the industry-standard spectra of interstellar dust by [15], with $R_V \equiv A_V/E(B-V) = 5.5$.

   A routine to interpolate the dust spectrum and calculate the extinction, as in that figure, is available on request. Figure 7 is an image of the extinction toward M 42, derived from MUSE data from the Balmer decrement.

2. **Determine the electron density and temperature.** The idea here is to base determination of one of the parameters mostly in a way that is insensitive to the other. For electron density, you need two lines of the same species whose upper states have similar energy but different critical densities, and not too different from the actual electron density, n_e. You get bonus points for using pairs of lines in which all states have energies $\ll kT$, such as the far-infrared lines among the ^{3}P states of O^{++}. In such cases, the results are nearly independent of T. For temperature, you need two lines of the same species for which the upper-state energies differ by at least a hefty fraction of kT, where T is the actual temperature.

   This process is illustrated well by **nomograms**: contours of line-intensity ratios, calculated with Equations 30 and 27, plotted in n_e–T space. Two example nomograms appear in Figure 8 and 9. With n_e on the horizontal axis, intensity ratios with nearly vertical contours are good for measuring n_e nearly independently of T, as with the visible [SII] 6717Å / 6731Å ratio and especially with the far-infrared [OIII] 51.82μm / 88.35μm ratio, for $n_e = 10^2$ cm^{-3} – 10^4 cm^{-3}. Intensity ratios with nearly horizontal contours are good for measuring T nearly independently of n_e, as with [SII] 1032 nm/671.7 nm at low densities and [OIII] 4363Å/5007Å up to $n_e \sim 10^5$ cm^{-3}.

   If a species has just three states in which all the population resides to good approximation, such as the ^{3}P states of O^{++} at densities below about 10^4 cm^{-3} (Figure 6), the three equations to which Equation 26 reduces have an easy algebraic solution for electron density [12]:

$$n_e = \frac{\gamma_{01}(A_{21}+A_{20}) + \gamma_{02}(A_{21}+rA_{10})}{\gamma(r\gamma_{12}-\gamma_{21}-\gamma_{20}) + \gamma_{02}(r[\gamma_{12}+\gamma_{10}]-\gamma_{21})} \tag{32}$$

   where $r = I_{10}\lambda_{10}A_{21}/I_{21}\lambda_{21}A_{10}$. Observations of forbidden lines in lowest-energy ^{3}P terms are highly prized for this property, despite being available only with relatively poor angular resolution.

   The MUSE observations of M 42 [14, 9] have been reduced in this fashion, in essence, by iteration of the following steps. From Equation 30, the authors determined the upper-state population fractions f_j and their uncertainties for pairs of lines with nearly vertical nomogram contours. Then, by solution to Equation 26, in the same manner as to produce Figure 6, they determined density n_e, and the uncertainty therein. Repeating the process for line pairs of the same species with nearly horizontal nomogram yields the temperature T. In the MUSE data set, the authors found a comforting close similarity in the density and temperature results for line pairs from species with different abundances and ionization state, which may be taken to indicate that the approximation of a uniform 1D slab for each pixel is pretty good.

   Sample results for density and temperature from the MUSE data analysis appear in Figures 10 and 11.

3. **Determine ionic and elemental relative abundances**. Once you know extinction, density, and temperature, you know everything but the column densities in Equation 30. The relative abundances are the ratios of column density, usually of an ionic line to a hydrogen recombination line. If the observations yield relative abundances for all significant ionization stages of a given element, you can obtain the relative abundances of that element. One of the cleanest examples of this sort of result is also one of the more astrophysically important: oxygen. O has an ionization potential very close to hydrogen's, 13.6 eV, so it is photoionized wherever hydrogen is. O^{++} has an ionization potential of 54.9 eV, too large even for hot O stars to produce abundantly in photon form. So images of the column densities $N_{O^+}, N_{O^{++}}$, and $N_p = N_{H^+}$ cover these species throughout most HII regions. Their ratios,

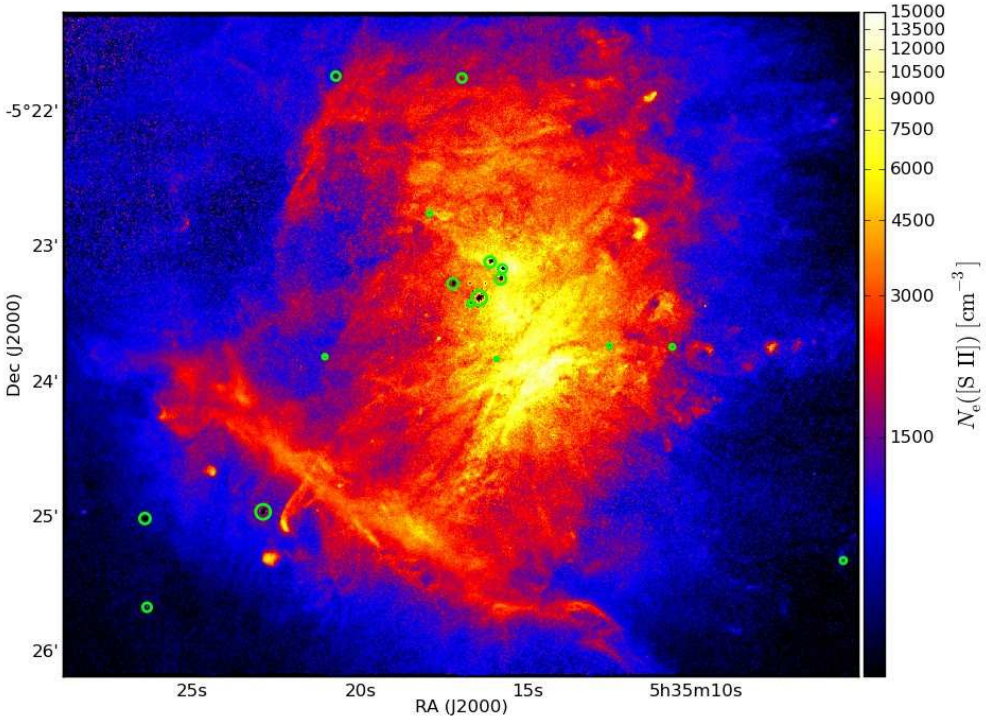

Figure 10: Image of electron density in M 42 [14], derived from images of [SII] 6717Å and 6731Å.

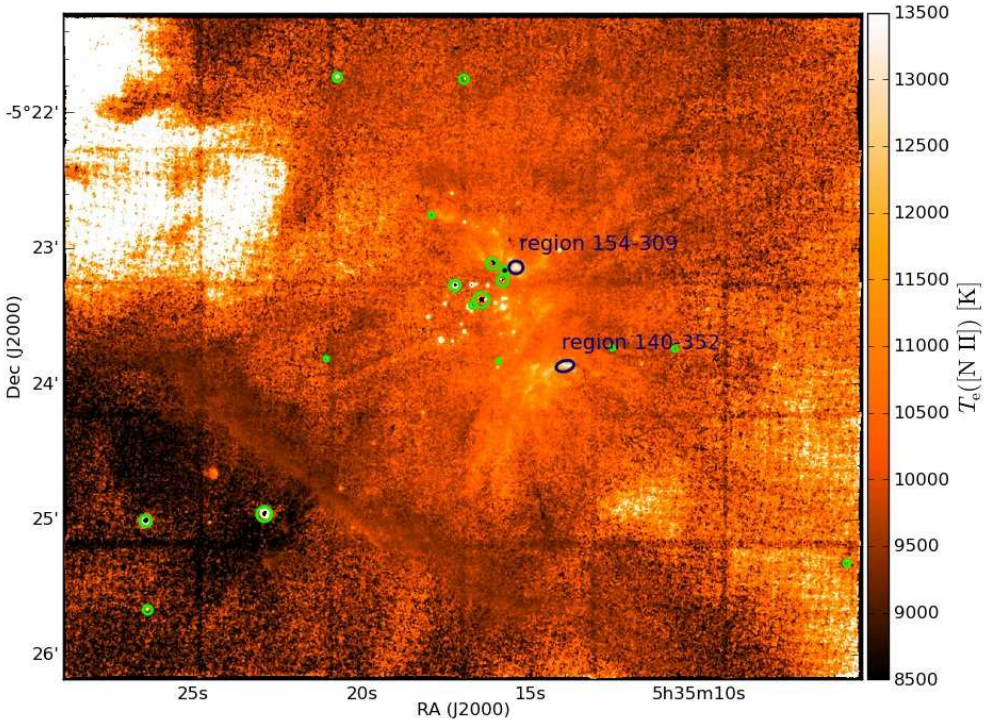

Figure 11: Image of temperature in M 42 [14], derived from images of [NII] 5755Å and 6548Å. N^+ and O^{++} are isoelectronic; these lines are the [NII] counterparts of [OIII]'s 4363Å and 5007Å lines.

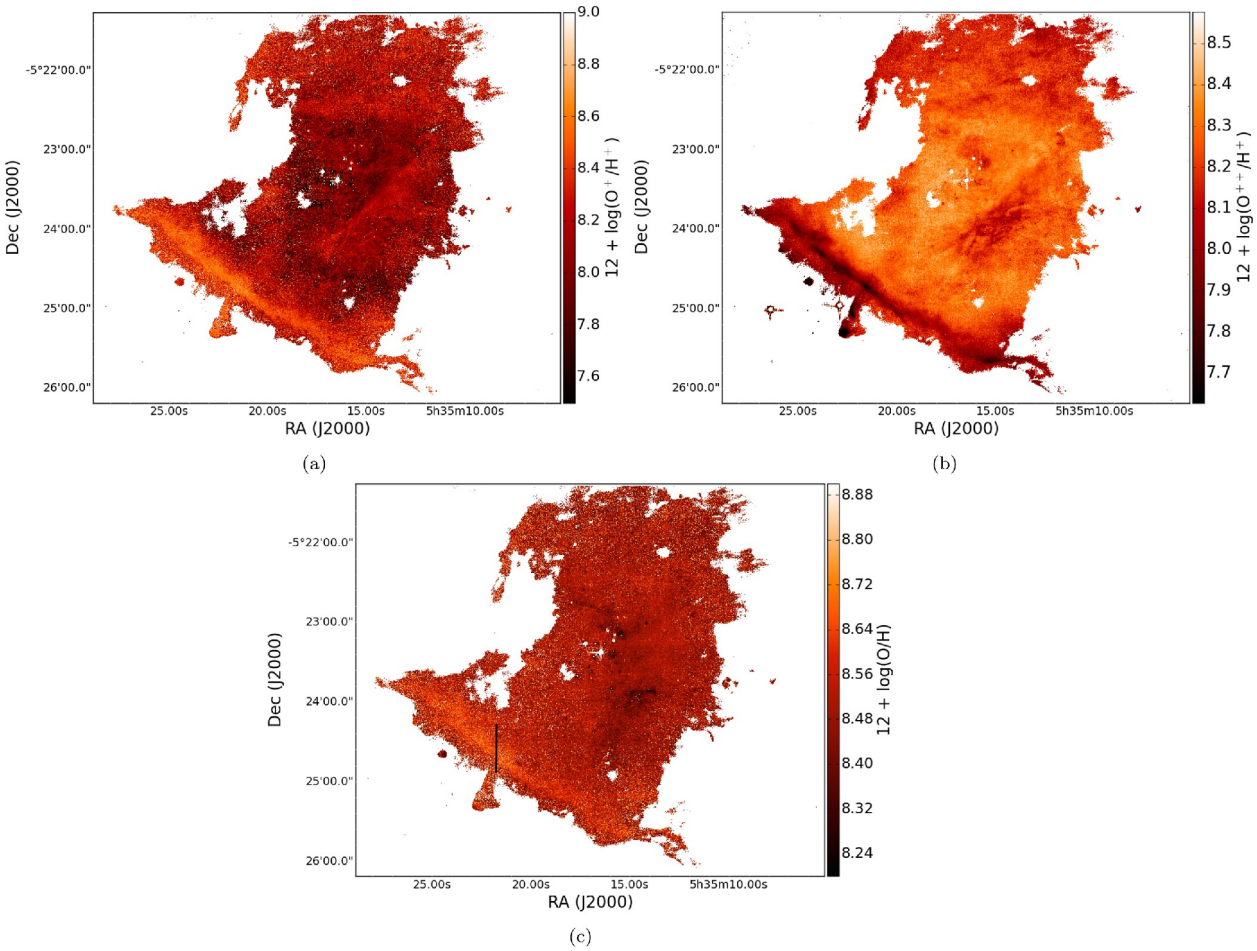

Figure 12: MUSE images of logarithms of oxygen abundance [9], from [OII], [OIII], and Hα, after extinction correction, density and temperature determination. O^+/H^+ at upper left, O^{++}/H^+ at upper right, O/H below.

O^+/H^+ and O^{++}/H^+ for short, are useful in constraining the properties of the O star which gives rise to the ionizing ultraviolet; this can be especially useful when the star suffers greater extinction than the spectral line emitting regions. The sum $O/H = O^+/H^+ + O^{++}/H^+$ is one of the most accurate oxygen relative abundances that money can buy.

Figures 12 and 13 are MUSE images [9] of the relative ionic and elemental abundances of oxygen and sulfur in M 42. Note that the higher ionization states tend to be more abundant closer to the four Trapezium stars, θ^1 Ori A–D, rather than the O stars on the other side of the bright bar, θ^2 Ori A–C. Thus, none of the three of θ^2 Ori A–C play a significant role in ionizing M 42. Note also that the elemental abundance images exhibit much less variation across M 42 than the ionic abundances.

4. **Determine the ionizing star's temperature**. Zanstra [16] was one of the first to apply quantum mechanics to the observations of nebulae to determine the stellar properties of the ionizing source of the nebulae. He assumed that the region is optically thick and composed entirely of hydrogen. By "optically thick,", he was assuming that every photon emitted by the star capable of ionizing a hydrogen atom would be absorbed by an atom in the nebula. He also assumed that the region is optically thin to the recombination lines, thereby allowing the assumption that every ionizing photon produced by the star is detected as one of the photons in the Balmer series.

   Using this assumption, we can equate the recombination rate to the number of ionizing photons emitted

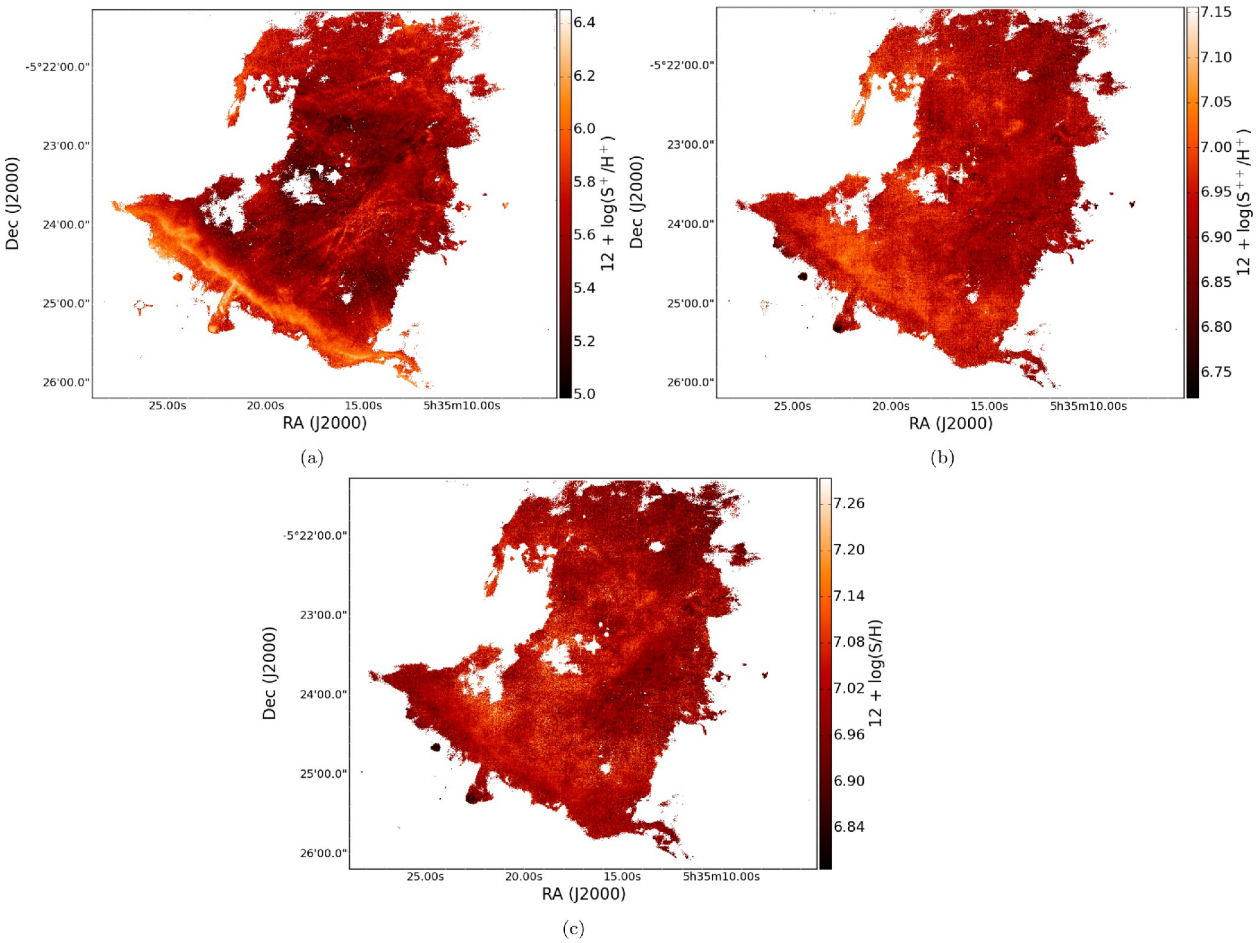

Figure 13: MUSE images of logarithms of sulfur abundance [9], from [SII], [SIII], and Hα, after extinction correction, density and temperature determination. S^+/H^+ at upper left, S^{++}/H^+ at upper right, S/H below.

by the star:

$$\int_{\nu_0}^{\infty} \frac{L_\nu}{h\nu}\, d\nu = \int n_p n_e \alpha_B\, dV \tag{33}$$

where $\alpha_B = 2.6 \times 10^{-13}$ cm^3/s is the case B recombination coefficient. We can use Eqn. 28 to eliminate the integral on the right-hand side, acquiring the relation

$$\frac{L_\nu}{\int_{\nu_0}^{\infty} \frac{L_\nu}{h\nu}\, d\nu} = h\nu \frac{\alpha_\nu}{\alpha_B} \tag{34}$$

Recalling the relationship between luminosity and flux, we find that

$$\frac{F_\nu}{\int_{\nu_0}^{\infty} \frac{f_\nu(T)}{h\nu}\, d\nu} = h\nu \frac{\alpha_\nu}{\alpha_B} \tag{35}$$

where $f\nu(T)$ is the flux emitted by a blackbody of temperature T,

$$f_\nu(T) = \int_\Omega B_\nu(\nu, T) \cos\theta\, d\Omega \tag{36}$$

10.2 More complex, 1D and 3D models

Nothing prevents you from using other things that you know about your target to generate more complex models — except, maybe, for the amorphous shape of most bright HII regions. 3D modeling goes better in compact HII regions — those found deeply embedded in molecular clouds, created by the youngest OB stars — and in planetary nebulae, both of which often appear at least axisymmetric, if not actually spherical. In either case, the procedure would be to dissect the structure into small blocks, within which the temperature, density, and ion abundances can be taken to be uniform and given by your model. Then, Equation 27 can be used to find the population fractions, and Equation 28 can be used to generate the spectral line intensities. Add extinction if you like. Embed all this in a routine in which n_e, T, and abundances are free parameters, to fit to observations.

There is also a virtue in considering a medium that differs from uniform by a small perturbation. A long time ago, Peimbert [11] found that fits to HII region specta improved when temperature fluctuations in a uniform medium were included. He characterized these fluctuations in terms of a temperature determination from a given line intensity ratio like [OIII] 4363Å/5007Å by modeling the intensity-to-temperature conversion with a power law, and then expanding in a Taylor series about the mean temperature. In this scheme, the first-order term is typically 10–20%, meaning that this is the amplitude of the perturbation. This worked well in the days that beam sizes were tens of arcsec in diameter. Nowadays, at least the components of these fluctuations in the plane of the sky are fully resolved in nearby HII regions, so the procedure is probably not as beneficial as it used to be, but it is still a useful tool for modeling more distant regions in this and other galaxies.

11 CHIANTI and Cloudy

Once you understand the basic principles elaborated above, you modelers of HII regions and planetary nebulae — you are one, now — can resort to two widely-used resources to reduce the work of assembling the necessary atomic-physical parameters and generating model HII region spectra.

CHIANTI[17] [5] is a comprehensive database of wavelengths, energies, A-coefficients, and collisional strengths calculated over a useful range of temperatures. The site includes all the atomic data, bundled into uniformly-formatted files, with links to the original publications of the calculations. It also includes code written in your choice of IDL or Python, to aid in accurate computation of upward and downward collisional rate coefficients from the collision strengths, and to make simple calculations of emitted spectra. A couple of versions ago, CHIANTI was adopted as the atomic-physics source for two industry-standard nebular codes, MAPPINGS for 1D shocks and Cloudy for photoionized regions. One might quibble with the

[17] www.chiantidatabase.org

calculations for e^-–Fe^+ collisions the CHIANTI-masters chose to include in the database, but the data are reliable in essentially all other respects. It saves an awful lot of work to have this standardized access to atomic data.

Cloudy[18] [6], invented by and with development still led by Gary Ferland, is a C++-based tool for synthesizing spectra of photoionized regions. It is one of the oldest and best documented openly-accessible simulation codes in astrophysics, and it is nicely interfaced to the leading database sources for atomic physics and stellar atmospheres. One of the most widely-used graduate-level astronomy textbooks, Osterbrock & Ferland's *Astrophysics of gaseous nebulae and active galactic nuclei* (2^{nd} edition, 2006, a.k.a. AGN3) can be regarded as Cloudy's user manual. It takes awhile to become an expert in Cloudy, but good results can be obtained long before rising to black-belt status. Highly recommended for anyone who deals with any of the subjects covered in AGN3, which is probably most of us.

References

[1] I. S. Bowen. The Origin of the Chief Nebular Lines. *PASP*, 39(231):295, October 1927.

[2] I. S. Bowen. The Origin of the Nebulium Spectrum. *Nature*, 120(3022):473, October 1927.

[3] I. S. Bowen. The Spectrum and Composition of the Gaseous Nebulae. *ApJ*, 81:1, January 1935.

[4] I. S. Bowen. The Image-Slicer a Device for Reducing Loss of Light at Slit of Stellar Spectrograph. *ApJ*, 88:113, September 1938.

[5] K. P. Dere, G. Del Zanna, P. R. Young, E. Landi, and R. S. Sutherland. CHIANTI—An Atomic Database for Emission Lines. XV. Version 9, Improvements for the X-Ray Satellite Lines. *ApJS*, 241(2):22, April 2019.

[6] G. J. Ferland, M. Chatzikos, F. Guzmán, M. L. Lykins, P. A. M. van Hoof, R. J. R. Williams, N. P. Abel, N. R. Badnell, F. P. Keenan, R. L. Porter, and P. C. Stancil. The 2017 Release Cloudy. *RMxAA*, 53:385–438, October 2017.

[7] D. G. Hummer and P. J. Storey. Recombination-line intensities for hydrogenic ions - I. Case B calculations for H I and He II. *MNRAS*, 224:801–820, February 1987.

[8] G. Kirchhoff. Ueber das Verhältniss zwischen dem Emissionsvermögen und dem Absorptionsvermögen der Körper für Wärme und Licht. *Annalen der Physik*, 185(2):275–301, January 1860.

[9] A. F. McLeod, P. M. Weilbacher, A. Ginsburg, J. E. Dale, S. Ramsay, and L. Testi. A nebular analysis of the central Orion nebula with MUSE. *MNRAS*, 455(4):4057–4086, February 2016.

[10] Cecilia H. Payne. Astrophysical Data Bearing on the Relative Abundance of the Elements. *Proceedings of the National Academy of Science*, 11(3):192–198, March 1925.

[11] Manuel Peimbert. Temperature Determinations of H II Regions. *ApJ*, 150:825, December 1967.

[12] J. W. V. Storey, D. M. Watson, and C. H. Townes. Observations of far-infrared fine structure lines: [O III] 88.35 microns and [O I] 63.2 microns. *ApJ*, 233:109–118, October 1979.

[13] P. J. Storey and Taha Sochi. The continuum emission spectrum of Hf 2-2 near the Balmer limit and the ORL versus CEL abundance and temperature discrepancy. *MNRAS*, 440(3):2581–2587, May 2014.

[14] Peter M. Weilbacher, Ana Monreal-Ibero, Wolfram Kollatschny, Adam Ginsburg, Anna F. McLeod, Sebastian Kamann, Christer Sandin, Ralf Palsa, Lutz Wisotzki, Roland Bacon, Fernando Selman, Jarle Brinchmann, Joseph Caruana, Andreas Kelz, Thomas Martinsson, Arlette Pécontal-Rousset, Johan Richard, and Martin Wendt. A MUSE map of the central Orion Nebula (M 42). *A&A*, 582:A114, October 2015.

[18] www.ublado.org

[15] Joseph C. Weingartner and B. T. Draine. Dust Grain-Size Distributions and Extinction in the Milky Way, Large Magellanic Cloud, and Small Magellanic Cloud. *ApJ*, 548(1):296–309, February 2001.

[16] H. Zanstra. An Application of the Quantum Theory to the Luminosity of Diffuse Nebulae. *ApJ*, 65:50, January 1927.